Available online at www.sciencedirect.com
ScienceDirect
International Journal of Heat and Mass Transfer 51 (2008) 2418–2432
International Journal of HEAT and MASS TRANSFER
www.elsevier.com/locate/ijhmt

Transient response of a planar participating medium subjected to a train of short-pulse radiation

R. Muthukumaran, Subhash C. Mishra *

Department of Mechanical Engineering, Indian Institute of Technology Guwahati, Guwahati 781039, India

Received 5 February 2007; received in revised form 6 August 2007
Available online 20 February 2008

Abstract

Transient response of a planar participating medium subjected to a short-pulse diffuse or collimated radiation is investigated. The pulse-width of the radiation is of the order of a nano-second. Short-pulse radiation can have a step or a Gaussian temporal variation. The homogenous participating medium with diffuse-gray boundaries is absorbing and scattering. The north boundary of the participating medium can be under the influence of a pulse train consisting of 1–4 pulses. The analysis is done using the finite volume method. Effects of the extinction coefficient and the scattering albedo on transmittance and reflectance signals are studied for a train of pulses. Unlike the previous studies with a single-pulse, a train of pulses provides more useful information about the medium.

1. Introduction

Thermal radiation being a part of the electromagnetic spectrum travels with the speed of light. In engineering applications, if the temporal evolutions of thermal quantities are desired at a time level as low as 10^{-9} to 10^{-15} s, transport of thermal radiation in a medium becomes a transient phenomenon. This situation occurs when an optically participating medium is subjected to a short-pulse radiation whose pulse-width too ranges from 10^{-9} to 10^{-15} s. The short-pulse radiation source gives rise to signals that too are short-spanned. They last for a time which is of the same order as that of the radiation source. These short-lived temporal signals depend upon the medium properties and thus they carry signatures of the medium. The temporal signatures have a wide range of engineering applications including but not limited to bio-medical diagnostics [1–7], fabrication of micro-devices [8], remote sensing of oceans and atmospheres [9,10], laser material processing of microstructures [11,12], particle detection and sizing [13] and fiber optic communications [14,15].

In the analysis of interaction of a short-pulse radiation with a participating medium, radiation is either diffuse [16–18] or collimated [16–31] and their temporal variations could either be a step [10–12,17,19–21,23,25,26,28,29,31] or a Gaussian function [19,20,24,27–30].

An interaction of a short-pulse radiation with a participating medium gives rise to temporal signals. In the previous studies [10–31] such temporal signals have mainly been analyzed with a single-pulse. However, a pulse train has potential applications in the emerging areas such as laser tissue welding and soldering [6], laser metal surface finishing, laser metal marking and engraving, nano-photonics [12], fiber optic communications [14,15], etc. Therefore, for enhanced information, a medium subjected to a train of pulses can be considered and the resulting thermal signals can be analyzed. The present work is therefore aimed at investigating the transport of a train of short-pulse radiation through a participating medium and analyzing the signals received at the boundaries.

In [17] Chai has studied the effect of a collimated step pulse train on a 1-D planar medium. He limited his study

* Corresponding author. Tel.: +91 361 2582660; fax: +91 361 2690762.
E-mail address: scm_iitg@yahoo.com (S.C. Mishra).

0017-9310/$ - see front matter © 2007 Elsevier Ltd. All rights reserved.
doi:10.1016/j.ijheatmasstransfer.2007.08.035

Nomenclature

a	anisotropy factor
c	speed of light
G	incident radiation
H	Heaviside function
I	intensity
I_b	blackbody intensity, $\frac{\sigma T^4}{\pi}$
$\hat{i}, \hat{j}, \hat{k}$	unit vectors in x-, y-, z-directions, respectively
M	number of discrete directions
p	scattering phase function
$\hat{n}$	outward normal
q	heat flux
S	source term
s	geometric distance in the direction of the intensity
T	temperature
T_p	time period of a pulse train
t	time
t_p	pulse-width
Z	physical depth of the medium
z	coordinate directions

Greek symbols

β	extinction coefficient
δ	Dirac-delta function
κ_a	absorption coefficient
μ	direction cosine with respect to the z-axis
ε	emissivity
θ	polar angle
σ	Stefan–Boltzmann constant $= 5.67 \times 10^{-8}$ W/m^2 K^4
σ_s	scattering coefficient
Ω	direction (θ, ϕ)
$\Delta\Omega$	solid angle, $\sin\theta \, d\theta \, d\phi$
ω	scattering albedo $\left(=\frac{\sigma_s}{\beta}\right)$
ϕ	azimuthal angle

Subscripts

c	collimated
d	diffuse
N, S	north, south
P	cell centre
r	reflectance
t	transmittance
w	wall/boundary

Superscripts

m	index for the discrete direction
*	dimensionless quantity

to temporal variations of the incident radiation inside the medium. Transmittance and reflectance signals at the boundaries which are detected by the instruments were not considered in his study. Further, his study was focused to a collimated step pulse and the effect of scattering albedo was not considered.

In the present work, the study with a train of pulses is generalized by presenting a formulation that is applicable for diffuse as well as collimated radiation having a step or a Gaussian temporal variation. Formulation is given for a 1-D planar participating medium. Temporal transmittance and reflectance signals are studied for different number of pulses. Effects of the extinction coefficient and the scattering albedo are considered. For the four combinations of radiation (diffuse and collimated) and temporal variations (step and Gaussian), transmittance and reflectance signals are analyzed.

In [26], Mishra et al. presented a general formulation for a single collimated step pulse and made a comparative study of the discrete transfer method, the discrete ordinate method and the finite volume method (FVM). They found that the results from the three methods were in good agreements with each other. The FVM is a more general method and is better adaptable to any geometry. Unlike the other two methods, it is less prone to ray effect. Therefore, in the present work, we have done the analysis using FVM. The details of the methodologies of the FVM used in the present work can be found in [26,32].

2. Formulation

The north boundary of the absorbing, emitting and scattering planar medium as shown in Fig. 1a and b is subjected to either a diffuse (Fig. 1a) or a collimated (Fig. 1b) short-pulse radiation. Temporal variations of radiation can either be a step (Fig. 1c) or a Gaussian function (Fig. 1d). The boundary can be under the influence of either a single or a train of pulses. The pulse-width t_p of the radiation is of the order of 10^{-9} s. The time interval between two consecutive pulses in the case of a pulse train is a multiple of t_p. To analyze the transmittance and the reflectance signals caused only by the short-pulse radiation, the homogeneous medium and its diffuse-gray boundaries are considered cold.

The incident pulse travels with the speed of light $c(=3 \times 10^8$ m/s). In case of the step-pulse (Fig. 1c), at any location in the medium, the part of the radiation source remains available for the duration of the pulse-width t_p. Whereas the Gaussian-pulse (Fig. 1d) remains available for the duration of $6t_p$. When the short-pulse radiation propagates through participating medium, the time-dependent diffuse radiation manifests and its life span in the medium is of the order of the pulse-width of the radiation source. In the present case in which radiation transport is a time-dependent phenomenon, the radiative transfer equation (RTE) in any direction $\hat{s}$ is given by [21,29,33]

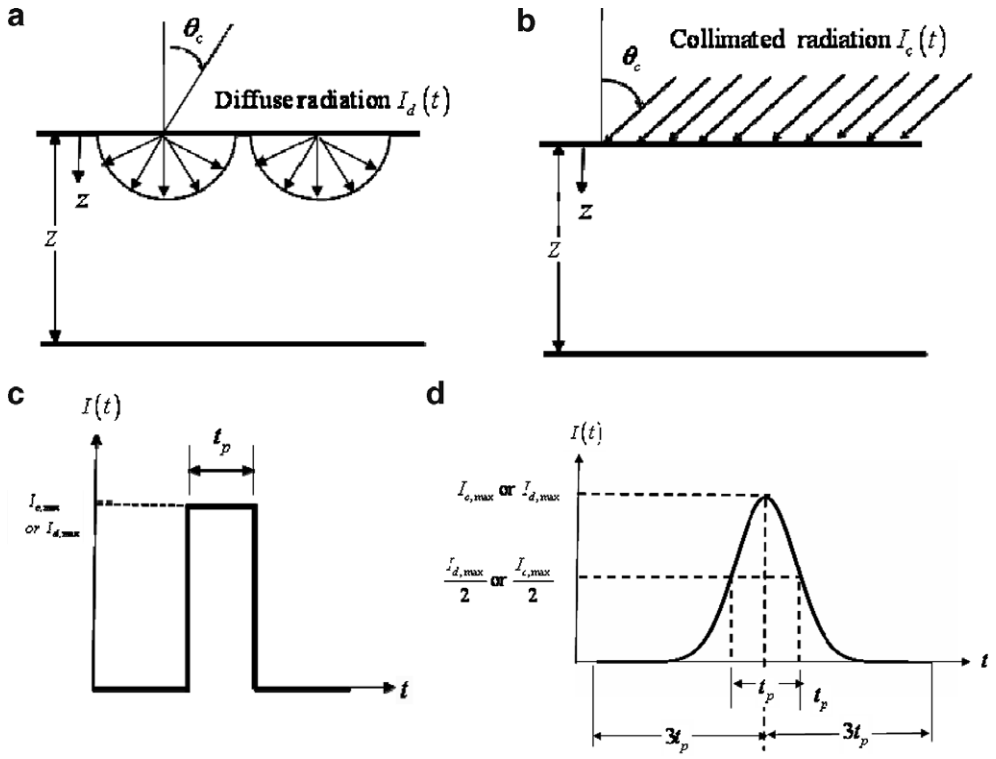

Fig. 1. A planar medium with its north boundary subjected to a short-pulse (a) diffuse radiation and (b) collimated radiation; (c) step and (d) Gaussian temporal profiles of diffuse and collimated radiations incident on the north boundary.

$$\left(\frac{1}{c}\right)\frac{\partial I}{\partial t}+\frac{\partial I}{\partial s}=-\beta I+\kappa_a I_b+\frac{\sigma_s}{4\pi}\int_{4\pi} I p(\Omega,\Omega')\,d\Omega' \tag{1}$$

where s is the geometric distance in the direction $\hat{s}=(\sin\theta\cos\phi)\hat{i}+(\sin\theta\sin\phi)\hat{j}+\cos\theta\hat{k}$, k_a is the absorption coefficient, β is the extinction coefficient, σ_s is the scattering coefficient and p is the scattering phase function.

Since in the present work, we are dealing with both diffuse as well as collimated radiation, in the following pages we provide a general formulation for the latter case. The changes in the formulation for the diffuse radiation will be highlighted wherever its need is felt.

When the collimated radiation encounters the medium and passes through it, its decay gives rise to the diffuse radiation. Thus within the medium, the intensity I is composed of two components, *viz.*, the collimated intensity I_c and the diffuse intensity I_d.

$$I=I_c+I_d \tag{2}$$

The variation of the collimated intensity I_c within the medium is given by

$$\left(\frac{1}{c}\right)\frac{\partial I_c}{\partial t}+\frac{\partial I_c}{\partial s}=-\beta I_c \tag{3}$$

Substituting Eq. (2) in Eq. (1), we get

$$\begin{aligned}\left(\frac{1}{c}\right)\frac{\partial I_c}{\partial t}+\frac{\partial I_c}{\partial s}+\left(\frac{1}{c}\right)\frac{\partial I_d}{\partial t}+\frac{\partial I_d}{\partial s}&=-\beta I_c-\beta I_d+\kappa_a I_b+\frac{\sigma_s}{4\pi}\int_{4\pi} I_d p(\Omega,\Omega')\,d\Omega'\\&\quad+\frac{\sigma_s}{4\pi}\int_{4\pi} I_c p(\Omega,\Omega')\,d\Omega'\end{aligned} \tag{4}$$

From Eqs. (3) and (4), we get

$$\left(\frac{1}{c}\right)\frac{\partial I_d}{\partial t}+\frac{\partial I_d}{\partial s}=-\beta I_d+S_c+S_d=-\beta I_d+S_t \tag{5}$$

where S_c and S_d are the source terms resulting from the collimated and the diffuse components of radiation, respectively. In Eq. (5), $S_t=S_c+S_d$ is the total source term. The source term S_c resulting from the collimated radiation I_c is given by

$$S_c(t)=\frac{\sigma_s}{4\pi}\int_{\Omega'=0}^{4\pi} I_c(\Omega,t)p(\Omega,\Omega')\,d\Omega' \tag{6}$$

For a linear anisotropic phase function $p(\Omega,\Omega')=1+a\cos\theta\cos\theta'$, the source term S_c in terms of the incident radiation G_c and heat flux q_c is written as

$$S_c(t)=\frac{\sigma_s}{4\pi}[G_c(t)+a\cos\theta q_c(t)] \tag{7}$$

Since the collimated intensity $I_c(\theta,t)$ for a step (Fig. 1c) and a Gaussian (Fig. 1d) pulse are defined by Eqs. (9) and (10), respectively, G_c and q_c in Eq. (7) are given by

$$G_c(t) = I_c(\theta, t) \tag{8a}$$
$$q_c(t) = I_c(\theta, t)\cos\theta \tag{8b}$$

$$I_c(\theta,t) = I_{c,\max}(\theta,t)\exp(-\beta s_c) \times [H\{\beta(ct - s_c)\} - H\{\beta(ct - s_c) - \beta c t_p\}] \times \delta(\theta - \theta_c) \tag{9}$$

$$I_c(\theta,t) = I_{c,\max}(\theta,t)\exp(-\beta s_c) \times \exp\left[-4\left(\frac{t - \frac{s_c}{c} - t_c}{t_p}\right)^2 \ln 2\right] \times \delta(\theta - \theta_c), \quad 0 < t < 2t_c \tag{10}$$

where in Eqs. (9) and (10), $I_{c,\max}$ is the collimated intensity at the north boundary, $s_c = z/\cos\theta_c$ is the geometric distance in the direction θ_c of the collimated radiation, δ is the Dirac-delta function and H is the Heaviside function defined as

$$H(y) = \begin{cases} 1, & y > 0 \\ 0, & y < 0 \end{cases} \tag{11}$$

In Eqs. (9) and (10), the Dirac-delta function δ takes care of existence of collimated radiation in θ_c direction while the Heaviside function H guarantees that the short-pulse radiation is available at any location in the medium only for the time duration t_p for a step function. Since the Gaussian-pulse is a continuous one, it is always available for the time span of $0 \leqslant t \leqslant 6t_p$ and the cut-off period $t_c = 3t_p$.

In case of a diffuse radiation (Fig. 1a), whose temporal variations could either be a step (Fig. 1c) or a Gaussian function (Fig. 1d), the diffuse intensity at the boundary is given by

$$I_d(\theta,t) = I_{d,\max}(\theta,t) \times [H(\beta ct) - H(\beta ct - \beta c t_p)] \tag{12}$$

$$I_d(\theta,t) = I_{d,\max}(\theta,t) \times \exp\left[-4\left(\frac{t - t_c}{t_p}\right)^2 \ln 2\right], \quad 0 < t < 2t_c \tag{13}$$

It is to be noted that Eqs. (9) and (10) are valid for all locations $0.0 \leqslant z \leqslant Z$ whereas Eqs. (12) and (13) are applicable to the boundary of incidence, in the present case $z = 0.0$, the north boundary. Equations governing the variation of the diffuse intensity $I_d(\theta, t)$ are given afterwards.

If $t^* = \beta ct, t_p^* = \beta c t_p$ and $t_c^* = \beta c t_c$ are the dimensionless times, Eqs. (9)–(13) can be written as

$$I_c(\theta,t^*) = I_{c,\max}(\theta,t^*)\exp(-\beta s_c) \times [H(t^* - \beta s_c) - H(t^* - \beta s_c - t_p^*)] \times \delta(\theta - \theta_c)$$

$$I_c(\theta,t^*) = I_{c,\max}(\theta,t^*)\exp(-\beta s_c) \times \exp\left[-4\left(\frac{t^* - \beta s_c - t_c^*}{t_p^*}\right)^2 \ln 2\right] \times \delta(\theta - \theta_c), \quad 0 < t^* < 2t_c^* \tag{14}$$

$$I_d(\theta,t^*) = I_{d,\max}(\theta,t^*) \times [H(t^*) - H(t^* - t_p^*)] \tag{15}$$

$$I_d(\theta,t^*) = I_{d,\max}(\theta,t^*) \times \exp\left[-4\left(\frac{t^* - t_c^*}{t_p^*}\right)^2 \ln 2\right], \quad 0 < t^* < 2t_c^* \tag{16}$$

In Eq. (5), for linear anisotropic phase function $p(\Omega, \Omega') = 1 + a\cos\theta\cos\theta'$, the source term S_d in terms of incident radiation G_d and heat flux q_d resulting from the diffuse radiation I_d is given by

$$S_d(t^*) = \kappa_a I_b(t^*) + \frac{\sigma_s}{4\pi}[G_d(t^*) + a\cos\theta q_d(t^*)] \tag{17}$$

In case of a planar medium in which radiation is azimuthally symmetric, G_d and q_d are given by and numerically computed from [32]

$$G_d(t^*) = 2\pi\int_{\theta=0}^{\pi} I_d(\theta,t^*)\sin\theta\,d\theta \approx 4\pi\sum_{k=1}^{M_\theta} I_d(\theta_k,t^*)\sin\theta_k\sin\left(\frac{\Delta\theta_k}{2}\right) \tag{18}$$

$$q_d(t^*) = 2\pi\int_{\theta=0}^{\pi} I_d(\theta,t^*)\cos\theta\sin\theta\,d\theta \approx 2\pi\sum_{k=1}^{M_\theta} I_d(\theta_k,t^*)\sin\theta_k\cos\theta_k\sin\Delta\theta_k \tag{19}$$

where M_θ is the number of discrete points considered over the complete span of the polar angle $\theta(0 \leqslant \theta \leqslant \pi)$.

For a boundary having temperature T_w and emissivity ε_w, the boundary intensity $I_d(r_w, t^*)$ is given by and computed from

$$I_d(r_w,t^*) \approx \frac{\varepsilon_w\sigma T_w^4}{\pi} + \left(\frac{1-\varepsilon_w}{\pi}\right)2\pi\sum_{k=1}^{M_\theta/2}[I_{d,w}(\theta_k,t^*) + I_{cw}(\theta_k,t^*)]\sin\theta_k\cos\theta_k\sin\Delta\theta_k \tag{20}$$

where in Eq. (20), the first and the second terms represent emitted and reflected components of the boundary intensity, respectively.

It is to be noted that if the boundary is subjected to only the diffuse radiation, in Eq. (20) $I_{c,w} = 0.0$.

In terms of non-dimensional time t^*, the RTE given in Eq. (5) is now written as

$$\beta\frac{\partial I_d}{\partial t^*} + \frac{\partial I_d}{\partial s} + \beta I_d = S_t \tag{21}$$

Using backward differencing scheme in time, Eq. (21) becomes

$$\beta\frac{I_d(t^*) - I_d(t^* - \Delta t^*)}{\Delta t^*} + \frac{\partial I_d(t^*)}{\partial s} + \beta I_d(t^*) = S_t(t^*) \tag{22}$$

Eq. (22) can be written in simplified form as

$$B\frac{\partial I_d(t^*)}{\partial s} + \beta I_d(t^*) = BS_t(t^*) + CI_d(t^* - \Delta t^*) \tag{23}$$

where $B = \frac{\Delta t^*}{(1+\Delta t^*)}$ and $C = \frac{\beta}{1+\Delta t^*}$.

With expressions for the source terms, incident radiation and heat flux given above, Eq. (23) is the resulting radiative transfer equation to be used in the present analysis.

Below we briefly present formulation and methodology to solve Eq. (23) using the FVM. Details of the FVM formulation for the steady-state radiative transfer in general can be found in Mishra and Roy [32] and for the transient radiation study, the same can be found in Mishra et al. [26].

Writing Eq. (23) for a discrete direction Ω^m and integrating it over the elemental solid angle $\Delta\Omega^m$, we get

$$B\int_{\Delta\Omega^m}\frac{\partial I_{\mathrm{d}}^m(t^*)}{\partial s}\,\mathrm{d}\Omega+\int_{\Delta\Omega^m}\beta I_{\mathrm{d}}^m(t^*)\,\mathrm{d}\Omega=\int_{\Delta\Omega^m}[BS_{\mathrm{t}}^m(t^*)+CI_{\mathrm{d}}^m(t^*-\Delta t^*)]\,\mathrm{d}\Omega \tag{24}$$

In case of a 1-D planar medium, Eq. (24) can be written as

$$B\frac{\partial I_{\mathrm{d}}^m(t^*)}{\partial z}D_z^m+\beta I_{\mathrm{d}}^m(t^*)=[BS_{\mathrm{t}}^m(t^*)+CI_{\mathrm{d}}^m(t^*-\Delta t^*)]\Delta\Omega^m \tag{25}$$

where D_z^m and $\Delta\Omega^m$ are given by

$$D_z^m=\left|\int_{\Delta\Omega^m}\cos\theta\,\mathrm{d}\Omega\right|=|2\pi\sin\theta^m\cos\theta^m\sin(\Delta\theta^m)| \tag{26}$$

$$\Delta\Omega^m=\int_{\Delta\Omega^m}\mathrm{d}\Omega=4\pi\sin\theta^m\sin\left(\frac{\Delta\theta^m}{2}\right) \tag{27}$$

Integrating Eq. (25) over the 1-D control volume ($\mathrm{d}V=1\times1\times\mathrm{d}z$) we get

$$[I_{\mathrm{d,N}}^m(t^*)-I_{\mathrm{d,S}}^m(t^*)]D_z^m=\left[-\frac{\beta}{B}I_{\mathrm{d,P}}^m(t^*)+S_{\mathrm{t,P}}^m+\frac{C}{B}I_{\mathrm{d,P}}^m(t^*-\Delta t^*)\right]\mathrm{d}z\Delta\Omega^m \tag{28}$$

where $I_{\mathrm{d,N}}^m$ and $I_{\mathrm{d,S}}^m$ are north and south control surface average intensities, respectively and $I_{\mathrm{d,P}}^m$ and $S_{\mathrm{t,P}}^m$ are the intensities and source terms at the cell centre P, respectively. In any discrete direction Ω^m, the cell-surface intensities are related to the cell-centre intensity $I_{\mathrm{d,P}}^m$ as

$$I_{\mathrm{d,P}}^m=\frac{I_{\mathrm{d,N}}^m+I_{\mathrm{d,S}}^m}{2} \tag{29}$$

From Eqs. (28) and (29), while marching from the north boundary for which $\theta<\frac{\pi}{2}$, we get

$$I_{\mathrm{d,P}}^m=\frac{\left[2D_z^mI_{\mathrm{d,N}}^m(t^*)+S_{\mathrm{t,P}}^m(t^*)dz\Delta\Omega^m+\left(\frac{C}{B}\,\mathrm{d}z\Delta\Omega^mI_{\mathrm{d,P}}^m(t^*-\Delta t^*)\right)\right]}{2D_z^m+\left(\frac{\beta}{B}\,\mathrm{d}z\Delta\Omega^m\right)} \tag{31a}$$

and while marching from the south boundary for which $\theta>\frac{\pi}{2}$, we get

$$I_{\mathrm{d,P}}^m=\frac{\left[2D_z^mI_{\mathrm{d,S}}^m(t^*)+S_{\mathrm{t,P}}^m(t^*)\,\mathrm{d}z\Delta\Omega^m+\left(\frac{C}{B}\,\mathrm{d}z\Delta\Omega^mI_{\mathrm{d,P}}^m(t^*-\Delta t^*)\right)\right]}{2D_z^m+\left(\frac{\beta}{B}\,\mathrm{d}z\Delta\Omega^m\right)} \tag{31b}$$

2.1. Solution procedure

The planar participating medium is discretized into a number of control volumes and the angular space, the polar angle θ is divided equally into a finite number of directions M_θ (Eqs. (18) and (19)). Calculation starts with a guess value of the source term $S_{\mathrm{t,P}}^m$ and the volume average diffuse intensity $I_{\mathrm{d,P}}^m(t^*-\Delta t^*)$ required for Eq. (31). For all the discrete directions for which $\theta<\frac{\pi}{2}$, marching starts from the north boundary and $I_{\mathrm{d,P}}^m(t^*)$ is calculated from Eq. (31a). The marching is done from the south boundary for all the directions for which $\frac{\pi}{2}<\theta<\pi$ and $I_{\mathrm{d,P}}^m(t^*)$ is calculated from Eq. (31b). For the control volume whose one boundary is the boundary of the medium, the boundary intensities required in Eq. (31) are calculated from Eq. (20). With $I_{\mathrm{d,P}}^m(t^*)$ calculated, the unknown cell-surface intensities in the same direction are calculated from Eq. (29). For the next control volume, the calculated cell-surface intensity serves as the known intensity in Eq. (31). The source term $S_{\mathrm{t,P}}^m=S_{\mathrm{c,P}}^m+S_{\mathrm{d,P}}^m$ is calculated from Eqs. (7) and (17). Collimated incident radiation G_{c} and heat flux q_{c} for $S_{\mathrm{c,P}}^m$ are computed from Eqs. (8a) and (8b), respectively and for the diffuse component $S_{\mathrm{d,P}}^m$, G_{d} and q_{d} are computed from Eqs. (18) and (19), respectively. All directions at a particular point are covered when marching is completed from both the boundaries. Before marching for the next time level, the maximum change in the source term $S_{\mathrm{t,P}}^m$ of a given control volume between the consecutive iteration levels are noted. Iteration is terminated when $|S_{\mathrm{t,old,P}}^m-S_{\mathrm{t,new,P}}^m|\leqslant1.0\times10^{-7}$. For any time t^*, reflectance and transmittance signals are computed from

$$\text{Reflectance}:\quad q_{\mathrm{r}}^*(0,t^*)=\frac{q_{\mathrm{d}}(0,t^*)}{q_{\mathrm{in}}(0,t^*)} \tag{32}$$

$$\text{Transmittance}:\quad q_{\mathrm{t}}^*(Z,t^*)=\frac{q_{\mathrm{c}}(Z,t^*)+q_{\mathrm{d}}(Z,t^*)}{q_{\mathrm{in}}(0,t^*)} \tag{33}$$

where in Eqs. (32) and (33), $q_{\mathrm{in}}(0,t^*)$ is the flux input to the medium through the north boundary. It should be noted that in Eqs. (32) and (33), reflectance $q_{\mathrm{r}}^*(0,t^*)$ and transmittance are the fluxes at the north and the south boundaries, respectively because of the contributions only from the medium.

3. Results and discussion

In the following pages, we consider the north boundary subjected to a single or a train of 2–4 diffuse and/or collimated pulses and analyze the time-dependent reflectance and transmittance signals that are basically the net heat fluxes on the north and the south boundaries, respectively. Temporal variations of these pulses could either be a step or a Gaussian function.

To validate the results, first we compare our results for a single-pulse with those available in the literature [26,30,33,34]. Next we present and analyze results for a train of pulses. This analysis is done for the range of values

of the extinction coefficient β and two values of the scattering albedo ω.

For grid independent results, 500 equal size control volumes were used and a maximum of 40 equally spaced directions in the polar space ($0 \leqslant \theta \leqslant \pi$) were found enough for the ray-independent solutions. 1000 divisions of the total time t^* domain were found sufficient for marching in the time dimension.

The code was written in Turbo C++. To study the computational time, the CPU times were recorded for all combinations of parameters. The code was executed on a Xeon 300 dual processor 800 MHz computer. The CPU times for optically thin ($\beta = 1.0$) to thick ($\beta = 5.0$) cases ranged from 36 s to 200 s, respectively.

3.1. Validation of results for a single-pulse

In this case, the north boundary of the planar medium is subjected to a single diffuse or a collimated pulse. Temporal variations of the pulse could either be a step or a Gaussian function. In Fig. 2a–d, for extinction coefficient $\beta = 0.5$ with scattering albedo $\omega = 1.0$ ($\omega = 0.998$ in Fig. 2d), transmittance $q_t^*(Z, t^*)$ results of the present work for a single-step diffuse, a single-step collimated and a single-Gaussian pulses are compared with those from the literature [26,30,33,34].

Whether radiation is diffuse or collimated, with a large step pulse, transient results approach steady state. Fig. 2a and b shows this for transmittance $q_t^*(Z, t^*)$ results for a large pulse-width $t_p^* = 25.0$ for a single-step diffuse and $t_p^* = 10.0$ for a single-step collimated pulses, respectively. Results have been compared with those from the literature [33,34]. Since with a Gaussian pulse, energy input to the medium is always changing, steady-state condition can never be approached for any value of the pulse-width t_p^*. For a single-step collimated and a single-Gaussian collimated pulses with $t_p^* = 1.0$, Fig. 2c and d provide comparison of our results with those from the literature [26,30], respectively. Results are in good agreement.

3.2. Results with a train of pulses

In the following pages, transmittance $q_t^*(Z, t^*)$ and reflectance $q_r^*(0, t^*)$ results with a train of pulses are provided for different values of the extinction coefficient β and the scattering albedo ω. In Figs. 3–10, these results are presented for pulse-width $t_p^* = 1.0$ and while dealing with collimated irradiation, its direction of incidence on the north boundary is considered to be normal, $\theta_c = 0.0$. In all the cases, the homogeneous medium is considered absorbing and isotropically scattering, and the diffuse-gray boundaries are black and cold. In the present work,

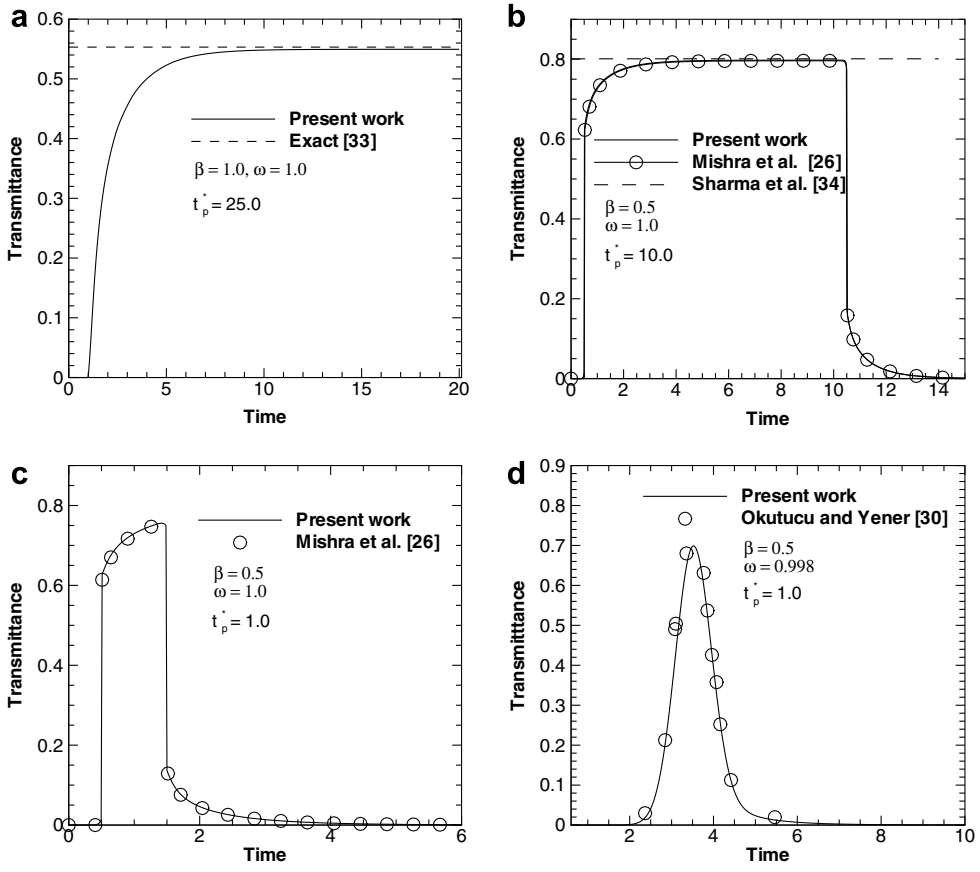

Fig. 2. Comparison of results: (a) step diffuse with a long pulse-width, (b) step collimated pulse with a long pulse-width, (c) step collimated pulse with pulse-width $t_p^* = 1.0$ and (d) Gaussian collimated pulse with pulse-width $t_p^* = 1.0$.

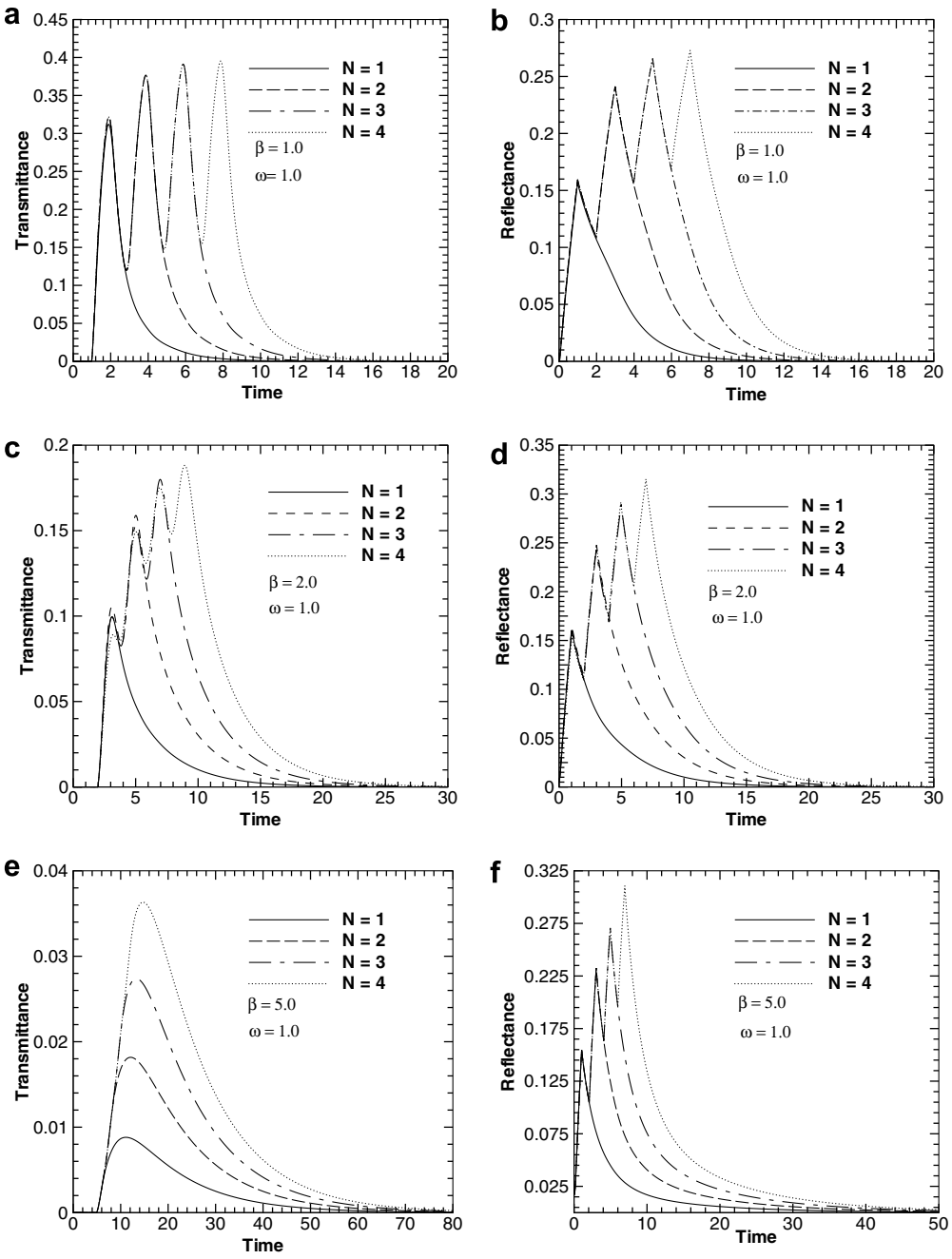

Fig. 3. Comparison of temporal variations of transmittance and reflectance signals for different values of the extinction coefficient β; Radiation source: diffuse step pulses.

transmittance and reflectance results have been provided for a medium whose physical depth $Z = 1$ m. However, it should be noted that the results presented are valid equally for any physical depth as long as for a given value the optical depth $\tau_Z = \beta Z$, the product of β and Z remains the same. For an example, results will be the same for $Z = 1.0$ m and $\beta = 1.0$ and $Z = 1/10$ m and $\beta = 10.0$ or any other combination of β and Z.

In all the cases of train of pulses considered in the present work, the pulses repeat after $t_p^* = 1.0$ and the north boundary is subjected to a maximum of four pulses. While considering the effect of the extinction coefficient β (Figs. 3–6), scattering albedo $\omega = 1.0$ and when considering the effect of the scattering albedo ω (Figs. 7–10) the extinction coefficient $\beta = 1.0$.

3.2.1. Effect of the extinction coefficient β

3.2.1.1. Diffuse step pulse train. The north boundary of the planar medium is subjected to diffuse radiation (Fig. 1a) whose temporal variation is a step function (Fig. 1c).

Fig. 3a–f show the effect of the extinction coefficient β for $N-$ pulses on transmittance $q_t^*(Z, t^*)$ and reflectance $q_r^*(0, t^*)$ signals, where $N = 1$–4. In these figures, results have been presented for extinction coefficient β=1.0, 2.0

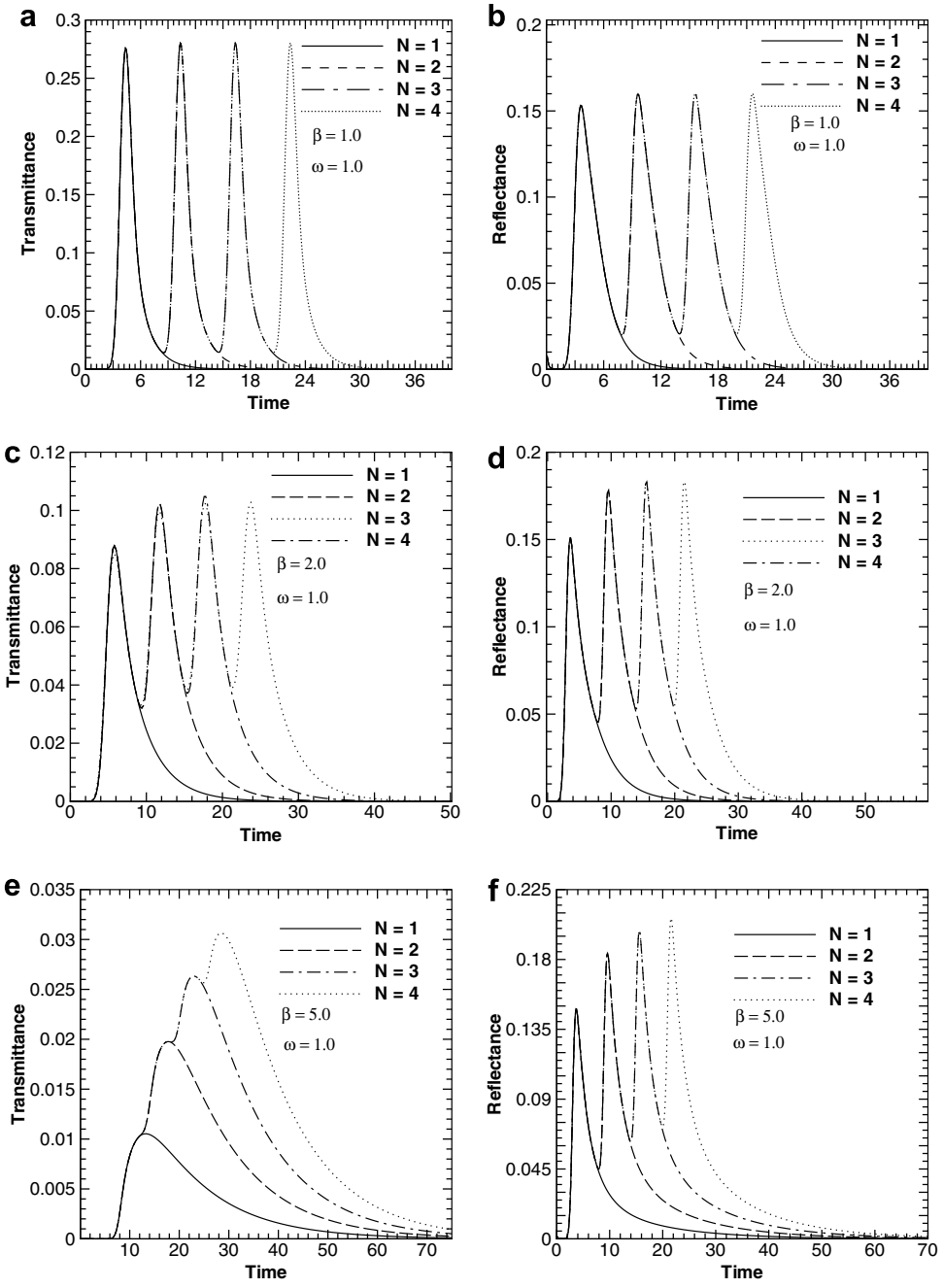

Fig. 4. Comparison of temporal variations of transmittance and reflectance signals for different values of the extinction coefficient β; radiation source: diffuse Gaussian pulses.

and 5.0. It is observed from the figure that for a single-pulse ($N = 1$), the magnitude of the transmittance $q_t^*(Z, t^*)$ signal decreases with increase in β. An opposite trend is observed for the reflectance $q_r^*(0, t^*)$ signal. Both the signals last longer for a higher value of β.

It is observed from Fig. 3a-d that when the medium is less participating ($\beta = 1.0$ and 2.0), with boundary subjected to N pulses, the $(N - 1)$ maxima of the transmittance $q_t^*(Z, t^*)$ and reflectance $q_r^*(0, t^*)$ signals occur almost at the same time as that of the $(N - 1)$ pulses. The same is the case with the minima. However, when the medium is highly participating ($\beta = 5.0$), for any number of pulses, only one maximum is present for the transmittance $q_t^*(Z, t^*)$ signals and the maximum of any pulse train is shifted slightly in time (Fig. 3e). Observation of Fig. 3a, c and e show that for $N \geqslant 2$, the difference in consecutive maximum and minimum decreases with increase in β. For $\beta = 5.0$, difference is not noticeable. In case of reflectance signals, maxima are always distinct.

A higher value of β signifies medium to be radiatively more participating and thus less amount of radiation reaches the bottom boundary, and consequently the

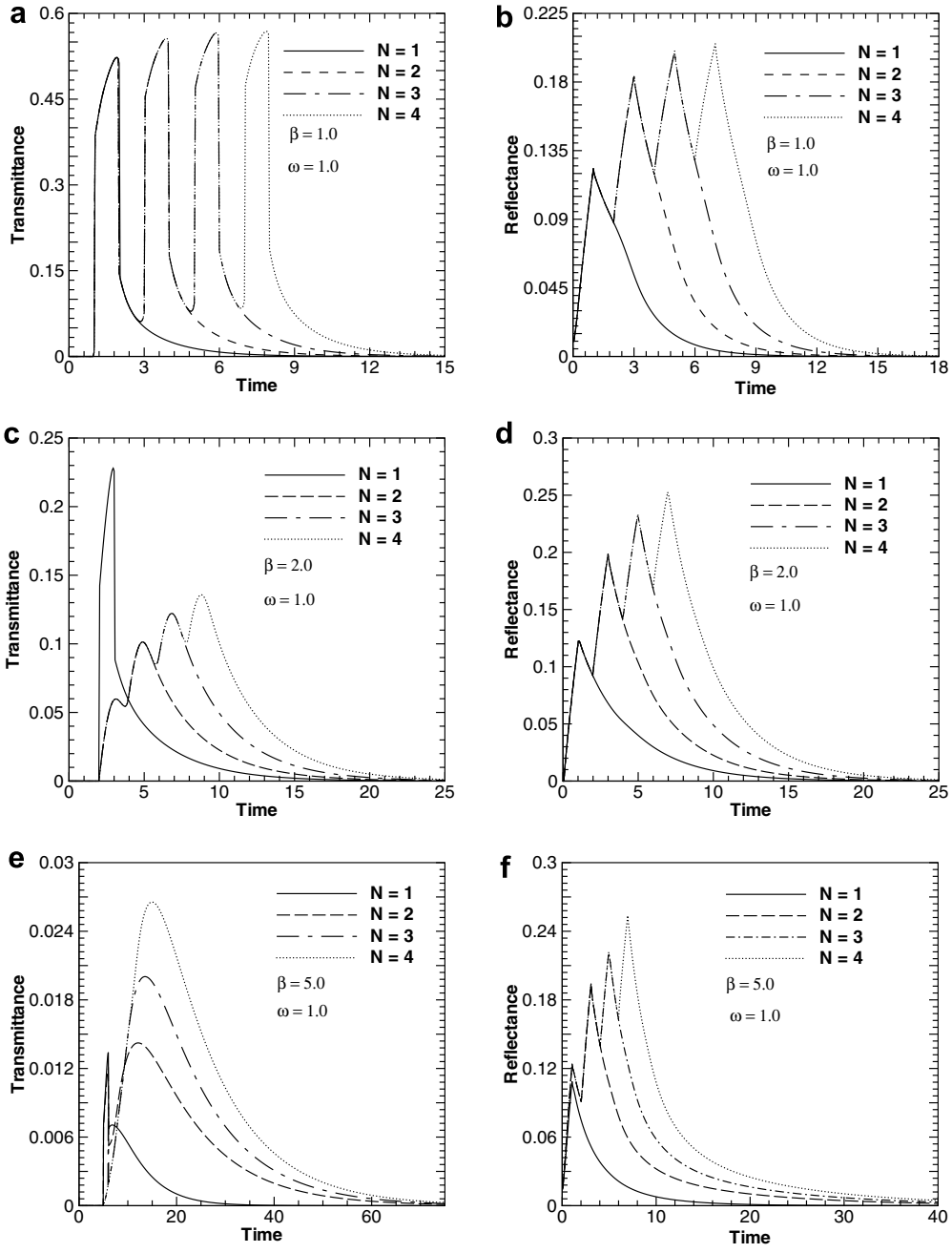

Fig. 5. Comparison of temporal variations of transmittance and reflectance signals for different values of the extinction coefficient β; radiation source: collimated step pulses.

magnitude of the transmittance $q_t^*(Z,t^*)$ signal decreases with increase in β. With increase in β, radiation stays for a longer duration in the medium and when the next pulse comes, radiation owing to previous pulses still remain present and this causes existence of multiple maxima and minima of transmittance $q_t^*(Z,t^*)$ and reflectance $q_r^*(0,t^*)$ signals for $N \geqslant 2$.

3.2.1.2. Diffuse Gaussian pulse train. The north boundary of the planar medium is subjected to diffuse radiation (Fig. 1a) whose temporal variation is a Gaussian function (Fig. 1d).

With $N = 1$–4, Fig. 4a–f show the effect of the extinction coefficient β=1.0, 2.0 and 5.0 on transmittance $q_t^*(Z,t^*)$ and reflectance $q_r^*(0,t^*)$ signals. It is observed that like the results of the diffuse step pulses, magnitudes of transmittance $q_t^*(Z,t^*)$ signals decrease with increase in β. Further because each pulse of the multiple Gaussian pulses remains available for time duration which is six times more than the step pulse, maxima are more widely spread over time. Further, like diffuse step pulses (Fig. 3e), for the same reason, for a higher value of the extinction coefficient ($\beta = 5.0$), multiple maxima and minima are not observed.

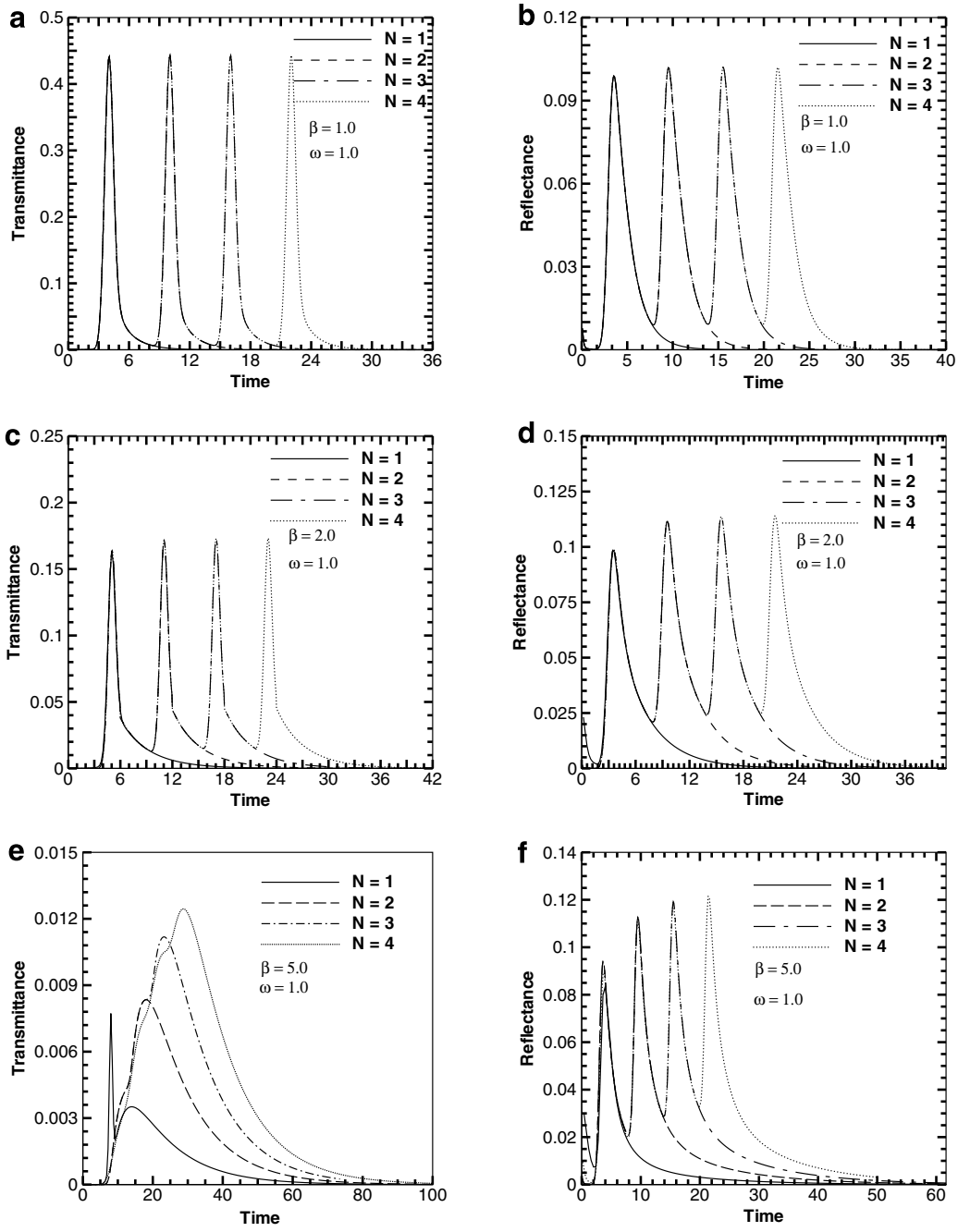

Fig. 6. Comparison of temporal variations of transmittance and reflectance signals for different values of the extinction coefficient β; radiation source: collimated Gaussian pulses.

In the case of Gaussian pulses, time span of a given pulse is six times more than that of the step pulse (Fig. 1c and d) and input too is very gradual. Thus, unlike step pulses (Fig. 3b, d, f), reflectance signals appear after some time (Fig. 4b, d, f). Distinct maxima and minima are observed. Because of more energy input to the medium and its existence for a longer duration at the boundary, transmittance $q_t^*(Z,t^*)$ and reflectance $q_r^*(0,t^*)$ signals in case of Gaussian pulses last longer (Fig. 4a–f) than that of step pulses (Fig. 3a–f).

3.2.1.3. Collimated step pulse train. The north boundary of the planar medium is subjected to collimated radiation (Fig. 1b) whose temporal variation is a step function (Fig. 1c). Angle of incidence θ_c of the collimated radiation is zero.

For $\beta = 1.0$, 2.0 and 5.0, Fig. 5a–f show the transmittance $q_t^*(Z,t^*)$ and reflectance $q_r^*(0,t^*)$ signals for $N = 1$–4 pulses Like the previous two cases, it is observed that the magnitudes of transmittance $q_t^*(Z,t^*)$ signals decrease and that of the reflectance $q_r^*(0,t^*)$ signals increases with

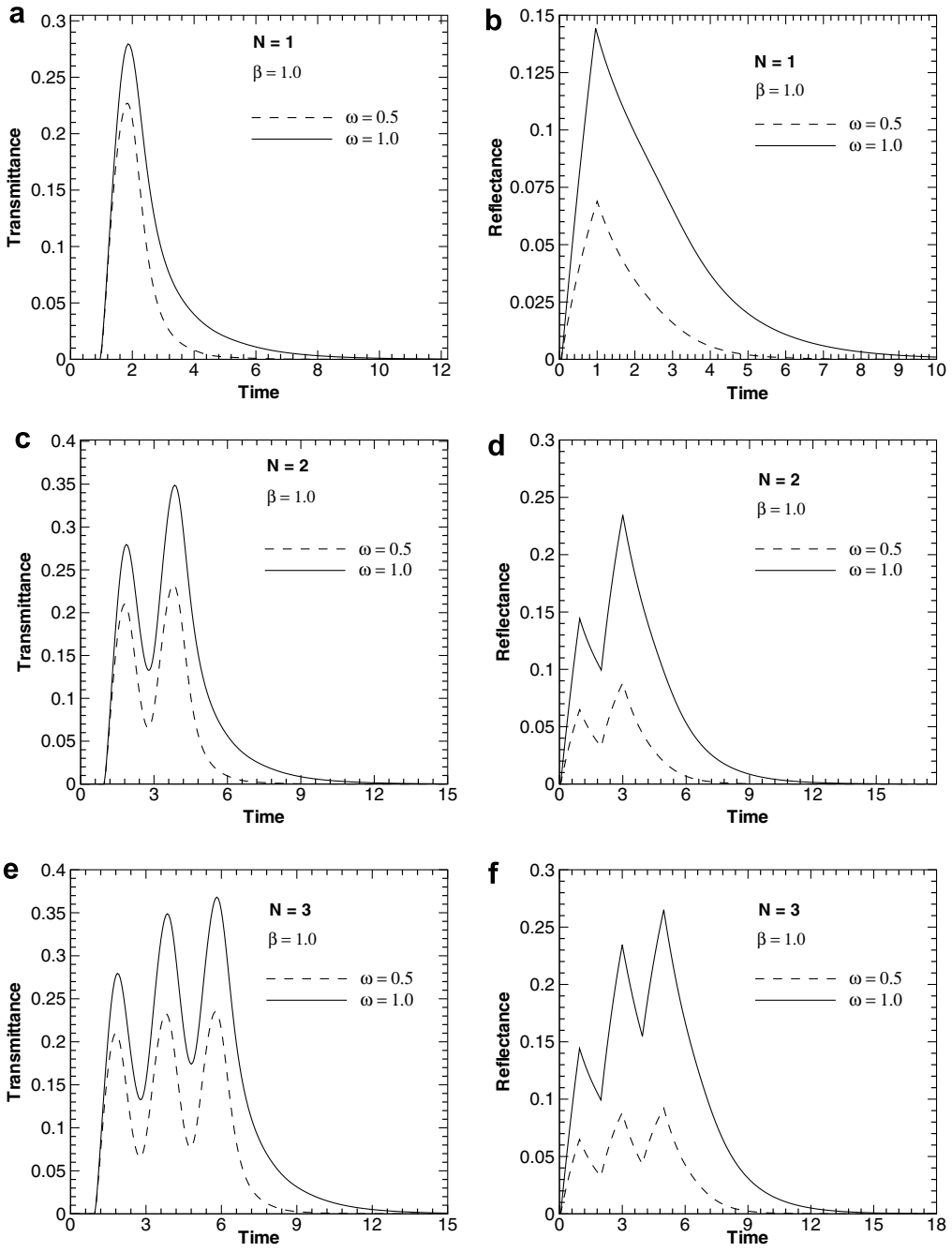

Fig. 7. Effect of scattering albedo ω on temporal variations of transmittance and reflectance signals; radiation source: diffuse step pulses.

increase in β. Distinct maxima and minima are observed with transmittance $q_t^*(Z,t^*)$ signals for lower values of β. However, for $\beta = 5.0$ (Fig. 5e), unlike diffuse step pulse trains (Fig. 3e), for $N \leqslant 3$, two distinct maximum and one minimum are observed. With increase in N, it is observed that the magnitude of the first maximum decreases and that of the second maximum increases. For $N = 4$, the first maximum and minimum disappear like all values of N in case of diffuse step pulses (Fig. 3e).

In case of a pulse train consisting of N pulses, radiation reaches the south boundary at time $t^* = \beta ct + NT_p^*$, where T_p^* is the time period. With a single collimated pulse, magnitudes of collimated and diffuse components are comparable, and thus for all values of β, distinct maximum in the transmittance $q_t^*(Z,t^*)$ signals is observed. When the number of pulses increase, in case of a higher value of β (Fig. 5e), because of the arrival of the successive pulses, the overall contribution of the collimated component decaying exponentially is dominated more by the diffuse component. Thus many maxima that are observed for lower values of β disappear at higher values of β.

Radiation enters the medium through the north boundary and thus this boundary receives radiation from the medium much earlier than the south boundary. Any

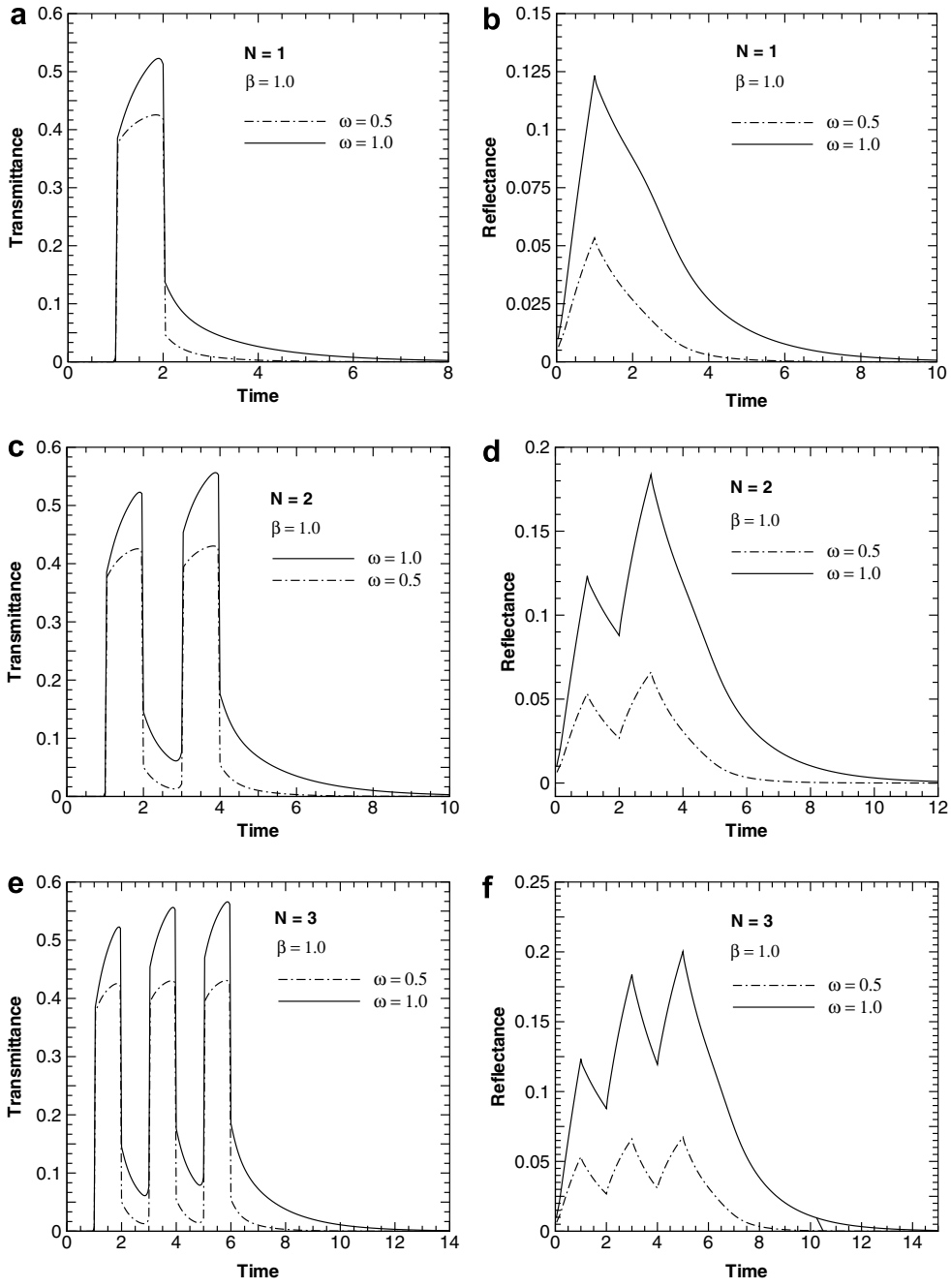

Fig. 8. Effect of scattering albedo ω on temporal variations of transmittance and reflectance signals; radiation source: collimated step pulses.

change in the input signal will be more noticeable on this boundary. Thus with the reflectance $q_r^*(0,t^*)$ signals, unlike transmittance $q_r^*(Z,t^*)$ signals, distinct peaks are observed for all values of β.

3.2.1.4. Collimated Gaussian pulse train. The north boundary of the planar medium is subjected to collimated radiation (Fig. 1b) whose temporal variation is a Gaussian function (Fig. 1d). Angle of incidence θ_c of the collimated radiation is zero.

For $\beta = 1.0$, 2.0 and 5.0, Fig. 6a–f show the transmittance $q_t^*(Z,t^*)$ and reflectance $q_r^*(0,t^*)$ signals for $N =$ 1–4 pulses. In comparison to diffuse Gaussian pulses (Fig. 4a–f), in this case, for $\beta = 1.0$, due to a higher collimated component, the magnitude of transmittance $q_t^*(Z,t^*)$ is much higher and also reflectance $q_r^*(0,t^*)$ signal is much lower due to the lesser contribution from the diffuse radiation. But as β increases to 5.0, the magnitudes of the maxima are less than that of the diffuse Gaussian pulses due to the fact that both the radiation source and the medium are highly diffusive in the latter case. The same reasoning can be attributed to the higher values of the reflectance that are observed in diffuse Gaussian pulses.

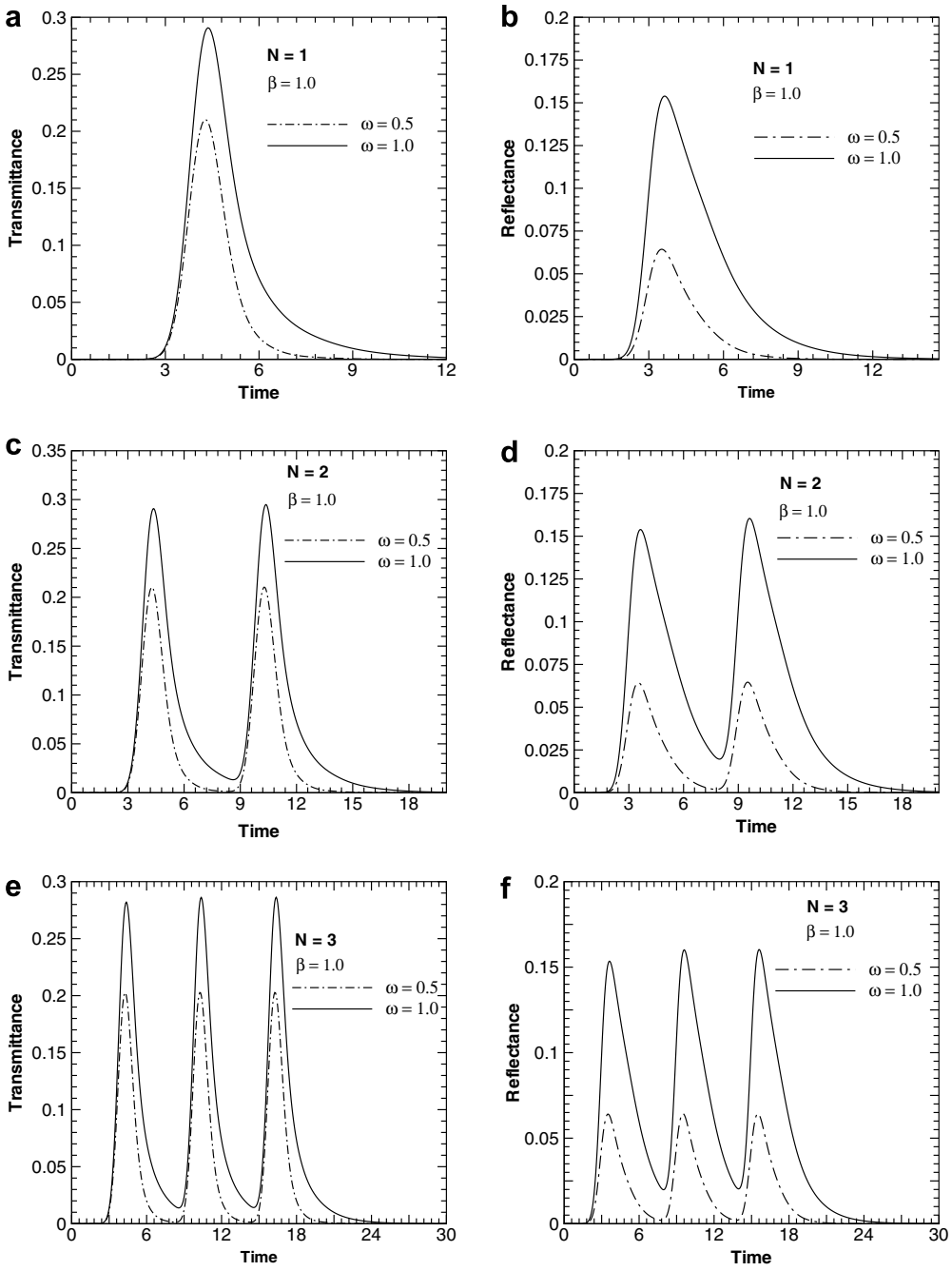

Fig. 9. Effect of scattering albedo ω on temporal variations of transmittance and reflectance signals; Radiation source: diffuse Gaussian pulses.

3.2.2. Effect of the scattering albedo ω

For the four cases described before, in Figs. 7–10, we now present the effect of the scattering albedo ω on transmittance $q_t^*(Z,t^*)$ and reflectance $q_r^*(0,t^*)$ signals for different pulse trains, $N=1$, 2 and 3. For the sake of legibility, unlike the effect of the β, here we compare the effects of ω for individual pulse trains. In all the cases, $\beta=1.0$ has been considered.

3.2.2.1. Diffuse step pulse train. For diffuse-step pulses, effects of ω on transmittance $q_t^*(Z,t^*)$ and reflectance $q_r^*(0,t^*)$ signals are presented in Fig. 7a–f. With decrease in ω, magnitudes of $q_t^*(Z,t^*)$ decrease. For all pulses, decrease is noticeable throughout and the changes are confined more towards maxima and minima. Scattering albedo ω is seen to have the same effect on $q_r^*(0,t^*)$. Further it is observed that ω is not having any effect on the time span of the signals.

3.2.2.2. Collimated step pulse train. For collimated step pulses, effects of ω on transmittance $q_t^*(Z,t^*)$ and reflectance $q_r^*(0,t^*)$ signals are given in Fig. 8a–f. In this case

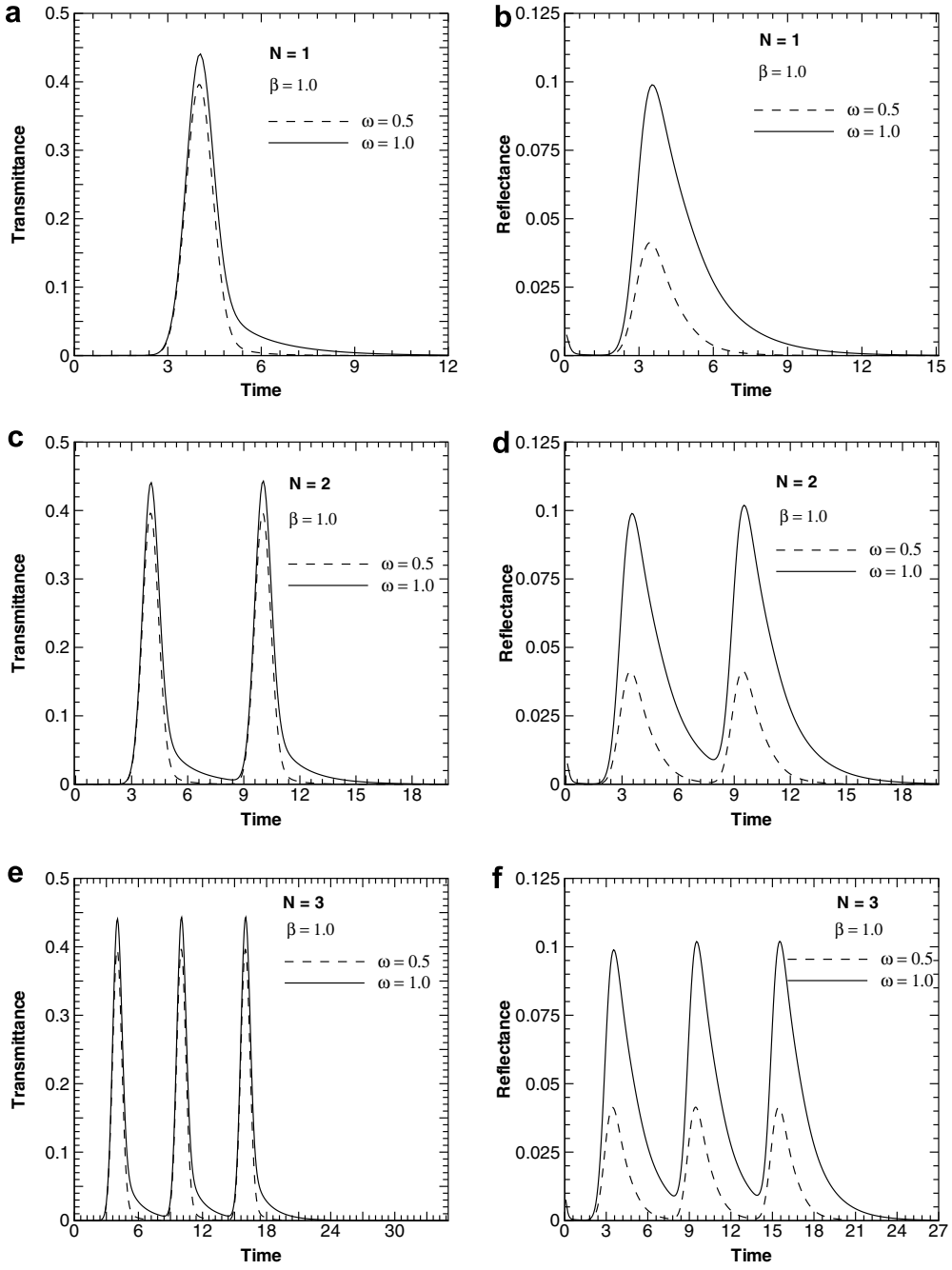

Fig. 10. Effect of scattering albedo ω on temporal variations of transmittance and reflectance signals; Radiation source: collimated Gaussian pulses.

too, for all values of N, magnitudes of both signals are less for lower value of ω. Effect of ω is more pronounced on the reflectance $q_r^*(0,t^*)$ signals.

3.2.2.3. Diffuse Gaussian pulse train. Effects of ω on $q_t^*(Z,t^*)$ and $q_r^*(0,t^*)$ signals for diffuse Gaussian pulses are given in Fig. 9a–f. Compared to diffuse step pulses (Fig. 7a–f), effect of ω in this case is more prominent on both types of signals.

For lower values of the scattering albedo ω, because of more absorption, a higher amount of radiation is trapped in the medium and accordingly in all the cases, both transmittance $q_t^*(Z,t^*)$ and reflectance $q_r^*(0,t^*)$ signals have lower magnitudes. The radiation decays as it travels towards the south boundary and ω will have less effect on $q_t^*(Z,t^*)$ in comparison to $q_r^*(0,t^*)$.

3.2.2.4. Collimated Gaussian pulse train. For collimated Gaussian pulse trains, effects of ω on transmittance $q_t^*(Z,t^*)$ and reflectance $q_r^*(0,t^*)$ signals are given in Fig. 10a–f. It is observed here that effects of ω on transmittance $q_t^*(Z,t^*)$ signals are less pronounced in comparison to reflectance $q_r^*(0,t^*)$ signals. Since β is less, the major amount of the energy received at the south boundary is

due to collimated component. Thus even as the radiation travels throughout the medium, the magnitude of ω which influences only the diffuse component is insignificant. But at the north boundary, the energy received being only due to the diffusive component, the difference due to the two values of $\omega = 1.0$ and 0.5, is felt distinctly.

4. Conclusions

Transient response of a planar absorbing–scattering medium subjected to a train of radiation pulses was analyzed. Four different combinations of diffuse and collimated radiation with step and Gaussian temporal variations were considered. Analysis was done using the finite volume method. Results for the train of pulses were first validated for a single-pulse with those available in the literature. Effects of the extinction coefficient and the scattering albedo were studied on transmittance and reflectance signals. For lower values of the extinction coefficient, distinct maxima and minima were observed in the signals of multiple pulses. With higher value of the extinction coefficient, multiple maxima in the transmittance signals were found to disappear. Scattering albedo was found to have relatively less effect on the transmittance signals. Signals were found to last for the same duration for the two values of the scattering albedo.

References

[1] F. Liu, K.M. Yoo, R.R. Alfano, Ultra-fast laser pulse transmission and imaging through biological tissues, Appl. Opt. 32 (1993) 554–558.

[2] Y. Yamada, Light-Tissue Interaction and Optical Imaging in Bio-Medicine, vol. 6, Beggel House, New York, 1995, p. 1–59.

[3] L.S. Bass, M.R. Treat, Laser tissue welding: a comprehensive review of current and future applications, Lasers Surg. Med. 17 (1995) 315–349.

[4] F.H. Loesel, F.P. Fisher, H. Suhan, J.F. Bille, Non-thermal ablation of neutral tissue with femtosecond laser pulses, Appl. Phys. B. 66 (1998) 121–128.

[5] M. Sakami, K. Mitra, T. Vo-Dinh, Analysis of short-pulse laser photon transport through tissues for optical tomography, Opt. Lett. 27 (2002) 336–338.

[6] K. Kim, Z. Guo, Ultrafast radiation heat transfer in laser tissue welding and soldering, Numer. Heat Transfer A 46 (2004) 23–40.

[7] S.K. Wan, Z. Guo, Correlative studies in optical reflectance measurements of cerebral blood oxygenation, J. Quant. Spectrosc. Radiat. Transfer 98 (2006) 189–201.

[8] V.V. Kancharla, S.C. Chen, Fabrication of biodegradable polymeric micro-devices using laser micromachining, Biomed. Microdevices 4 (2002) 105–109.

[9] R.E. Walker, J.W. Mclean, Lidar equation for turbid media with pulse stretching, Appl. Opt. 38 (1999) 2384–2397.

[10] K. Mitra, J.H. Churnside, Transient radiative transfer equation applied to oceanographic lidar, Appl. Opt. 38 (1999) 889–895.

[11] S. Kumar, K. Mitra, Microscale aspects of thermal radiation transport and laser applications, Adv. Heat Transfer 33 (1999) 187–294.

[12] L. Jiang, H.L. Tsai, Repeatable nanostructures in dielectrics by femtosecond laser pulse trains, Appl. Phys. Lett. 87 (2000), doi:10.1063/1.2093935.

[13] K.J. Grant, J.A. Piper, D.J. Ramsay, K.L. Williams, Pulse lasers in particle detection and sizing, Appl. Opt. 33 (1993) 416–417.

[14] A.D. Kim, J.N. Kutz, D.J. Muraki, Pulse-train uniformity in optical fiber lasers passively mode-locked by nonlinear polarization rotation, IEEE J. Quant. Electron. 36 (2000) 465–471.

[15] C.M. Ngabireng, P.T. Dinda, K. Nakkeeran, P.K.A. Wai, Radiating and non-radiating trains of light pulses in dispersion-managed optical fiber systems, Opt. Commun. 250 (2005) 24–35.

[16] Z. Guo, S. Kumar, Radiation element method for hyperbolic radiative transfer in plane-parallel inhomogeneous media, Numer. Heat Transfer B 39 (4) (2001) 371–387.

[17] J.C. Chai, One-dimensional transient radiative heat transfer modeling using a finite volume method, Numer. Heat Transfer B 44 (2003) 187–208.

[18] J.C. Chai, P.F. Hsu, Y.C. Lam, Three-dimensional transient radiative transfer modeling using the finite volume method, J. Quant. Spectrosc. Radiat. Transfer 86 (2004) 299–313.

[19] K. Mitra, M.S. Lai, S. Kumar, Transient radiation transport in participating media within a rectangular enclosure, J. Thermophys. Heat Transfer 11 (1997) 409–414.

[20] K. Mitra, S. Kumar, Development and comparisons of models for light-pulse transport through scattering-absorbing media, Appl. Opt. 38 (1999) 188–196.

[21] Z.M. Tan, P.F. Hsu, An integral formulation of transient radiative transfer, J. Heat Transfer 123 (2001) 466–475.

[22] Z.M. Tan, P.F. Hsu, Transient radiative transfer in three-dimensional homogeneous and non homogeneous participating media, J. Quant. Spectrosc. Radiat. Transfer 73 (2002) 181–194.

[23] C.Y. Wu, S.H. Wu, Integral equation formulation for transient radiative transfer in an anisotropically scattering medium, Int. J. Heat Mass Transfer 122 (2000) 818–822.

[24] C.Y. Wu, N.R. Ou, Differential approximation for transient radiative transfer through a participating medium exposed to collimated radiation, J. Quant. Spectrosc. Radiat. Transfer 73 (2002) 111–120.

[25] P. Rath, S.C. Mishra, P. Mahanta, U.K. Saha, K. Mitra, Discrete transfer method applied to transient radiative problems in participating medium, Numer. Heat Transfer A 44 (2003) 183–197.

[26] S.C. Mishra, P. Chug, P. Kumar, K. Mitra, Development and comparison of the DTM, the DOM and the FVM formulations for the short-pulse laser transport through a participating medium, Int. J. Heat Mass Transfer 49 (2006) 1820–1832.

[27] Z. Guo, J. Aber, B.A. Garetz, S. Kumar, Monte Carlo simulation and experiments of pulsed radiative transfer, J. Quant. Spectrosc. Radiat. Transfer 73 (2002) 159–168.

[28] Z. Guo, S. Kumar, Discrete-ordinates solution of short-pulsed laser transport in two-dimensional turbid media, Appl. Opt. 40 (2001) 3156–3163.

[29] M. Sakami, K. Mitra, P.F. Hsu, Analysis of light-pulse transport through two-dimensional scattering and absorbing media, J. Quant. Spectrosc. Radiat. Transfer 73 (2002) 169–179.

[30] T. Okutucu, Y. Yener, Radiative transfer in participating media with collimated short-pulse Gaussian irradiation, J. Phys. D: Appl. Phys. 39 (2006) 1976–1983.

[31] T. Okutucu, Y. Yener, A.A. Busnaina, Transient radiative transfer in participating media with pulse-laser irradiation – an approximate Galerkin solution, J. Quant. Spectrosc. Radiat. Transfer 103 (2007) 118–130.

[32] S.C. Mishra, H.K. Roy, Solving transient conduction–radiation problems using the lattice Boltzmann method and the finite volume method, J. Comput. Phys. 223 (2007) 89–107.

[33] M.F. Modest, Radiative Heat Transfer, second ed., Academic Press, New York, 2003.

[34] D.J. Sarma, S.C. Mishra, P. Mahanta, Analysis of collimated radiation using the discrete transfer method, J. Quant. Spectrosc. Radiat. Transfer 96 (2005) 123–135.